Anti-Windup Robust Backstepping Control for an Underactuated Reusable Launch Vehicle

Linqi Ye, Bailing Tian, *Member, IEEE*, Houde Liu, *Member, IEEE*, Qun Zong, *Member, IEEE*, Bin Liang, *Senior Member, IEEE*, and Bo Yuan, *Senior Member, IEEE*

***Abstract*—The attitude control of an underactuated reusable launch vehicle (RLV) in the reentry phase involving nonminimum phase problem and control input constraints is investigated in this article. To address the nonminimum phase problem, an approach combining output redefinition and robust backstepping is proposed, where a synthetic output is constructed using the combination of the original output and the internal states to obtain stable zero dynamics, and then robust backstepping is performed on the new output. Besides, the ideal internal dynamics are obtained by using optimal bounded inversion, which are incorporated into the controller as the reference trajectories for the internal states to improve the output tracking accuracy. To cope with the control input constraints, a simple and useful anti-windup strategy is proposed by using feedback error clipping, which is shown to be very effective in mitigating control input saturation. Numerical simulations are given to validate the effectiveness of the proposed method.**

***Index Terms*—Anti-windup, nonminimum phase, output redefinition, reusable launch vehicle (RLV), robust backstepping, underactuated.**

I. Introduction

LAUNCH vehicle system is an important technology which can send human and payload into earth orbit as well as outer space. In the past decades, scientists are making great efforts to cut down the cost, leading to the birth of reusable launch vehicles (RLVs). An RLV is usually launched into orbit by a rocket and it can reenter the atmosphere and return to the ground for the next use. From the space shuttle to the X-33 spaceplane, the crew return vehicle X-38, and the recent Falcon heavy rocket, RLVs have shown great potential to provide an economic way to enter space in the future.

During the reentry phase, an RLV flies like a glider which has poor maneuverability, in which its attitude is controlled by aerodynamic surfaces and a reaction control system (RCS). The attitude dynamics of an RLV are characterized by high nonlinearities, strong couplings, fast time-varying, and large uncertainties, making it a great challenge to design flight control systems. In recent years, several nonlinear control methods have been applied to the attitude control of RLVs. The most notable is sliding mode control, which is robust to model uncertainties. Various sliding mode control methods have been applied to control RLVs, such as high-order sliding mode [1], adaptive multivariable sliding mode [2], twisting sliding mode [3], and super-twisting sliding mode [4], just name a few. Another powerful nonlinear control method, backstepping, has also shown a good capability to handle the complicated RLV dynamics [5]–[7]. Besides, fuzzy control [8] and neural network control [9], [10] are also developed for RLVs, which can identify the system model and does not rely on exact model knowledge. Other methods, such as prescribed performance control [11], [12], trajectory linearization control [13], coupling characterization-based control [14], [15], and fault-tolerant control [16]–[18] are also studied.

However, all the aforementioned methods are based on the assumption that an RLV can generate moments about all three body axes, neglecting the fact that an RLV may experience limited control authority during certain reentry phase. Take X-38 as an example, which experiences a significant portion when the dynamic pressure is greater than 1500 Pa and the Mach number is more than 6, during which the vehicle is underactuated since the RCS thrusters are no longer available and the rudders are not yet been used [19]–[21]. During this period, an RLV has more outputs than the available inputs, that is, the angle of attack, the sideslip angle, and the bank angle are controlled by only two body flaps.

Future RLVs with lifting-body configurations are likely to bring about similar underactuated issues as those posed by X-38. As shown in [21] and [22], an underactuated RLV exhibits nonminimum phase behavior, which means the system has unstable zero dynamics. When applying traditional nonlinear control methods to the system without stabilizing the internal dynamics, the closed-loop system will exhibit

Manuscript received January 19, 2020; revised June 14, 2020; accepted August 15, 2020. Date of publication September 17, 2020; date of current version February 17, 2022. This work was supported in part by the National Natural Science Foundation of China under Grant 61803221, Grant U1813216, Grant 61673294, Grant 61773278, and Grant 61873340; in part by the Guangdong Young Talent with Scientific and Technological Innovation under Grant 2019TQ05Z111; and in part by the Interdisciplinary Research Project of Graduate School of Shenzhen of Tsinghua University under Grant JC2017005. This article was recommended by Associate Editor G. Pandey. *(Corresponding authors: Bailing Tian; Houde Liu.)*

Linqi Ye, Houde Liu, and Bo Yuan are with the Center for Artificial Intelligence and Robotics, Tsinghua Shenzhen International Graduate School, Tsinghua University, Shenzhen 518055, China (e-mail: ye.linqi@sz.tsinghua.edu.cn; liu.hd@sz.tsinghua.edu.cn; yuanb@sz.tsinghua.edu.cn).

Bailing Tian and Qun Zong are with the School of Electrical and Information Engineering, Tianjin University, Tianjin 300072, China (e-mail: bailing_tian@tju.edu.cn; zongqun@tju.edu.cn).

Bin Liang is with the Navigation and Control Research Center, Department of Automation, Tsinghua University, Beijing 100084, China (e-mail: bliang@tsinghua.edu.cn).

Color versions of one or more figures in this article are available at https://doi.org/10.1109/TSMC.2020.3020365.

Digital Object Identifier 10.1109/TSMC.2020.3020365

unsatisfactory oscillations or even lose stability. Obviously, this is unacceptable since it may cause severe flight accidents. Therefore, to guarantee flight safety, it is necessary to take measures to deal with the nonminimum phase problem. Due to the nonminimum phase property, it becomes extremely difficult to achieve high-precision trajectory tracking control while maintaining internal stability, which brings a great challenge to the control of underactuated RLVs. To date, only several results are given in the literature for this problem, including an output redefinition controller [21], a dynamic sliding mode controller [22], and an output feedback controller [23]. The methods in [21]–[23] have ensured the stability of an RLV in the underactuated case. However, it is noticed that none of them have incorporated the ideal internal dynamics (IIDs) into the controller ([21] only applies IID for constant commands). Since IID is the key to achieving accurate tracking for nonminimum phase systems [24], the methods in [21]–[23] may have degraded performance when applied to track practical guidance commands, which are time-varying signals.

Inspired by [21]–[24], the motivation of this article is to propose an improved controller for an underactuated RLV that can achieve accurate output tracking for time-varying signals. To achieve this goal, a method called optimal bounded inversion, which was proposed in our previous work [25], is used to obtain the IID and the controller is developed by combing output redefinition and robust backstepping. The advantages of the proposed method over existing ones are twofold. First, backstepping simplifies the controller design compared with [21]–[23] because there is no need to calculate the second-order derivative of the outputs and it can deal with both matched and mismatched disturbances. Second, the IID is incorporated into the controller of an underactuated RLV for the first time, which greatly improves the output tracking accuracy for time-varying signals.

Another realistic consideration is the control input constraint. The deflection of the aerodynamic surface has physical limits, which puts input constraints on the flight control system. An underactuated RLV is more sensitive to input constraints due to reduced control authority, which must be taken into account during controller design. A simple way to deal with control input constraints is to limit the magnitude of the calculated control input within its physical boundaries. However, this input clipping method may cause control input saturation. When this occurs, the system may lose control and induce instability. To solve this problem, various methods have been proposed, such as constrained adaptive backstepping [6], [26] and an auxiliary system method [7]. A common feature in these methods is that they introduce an additional system to adjust the control input when saturation occurs. The additional system makes the control law more complicated, which may limit their application in practice. In this article, a simple and effective anti-windup strategy is developed to handle control input constraints by using feedback error clipping. Unlike input clipping, the approach here puts limits on the magnitude of the feedback error rather than the control input. By limiting the feedback error in a relatively small bound, a smaller input is generated, and input saturation can thus be avoided.

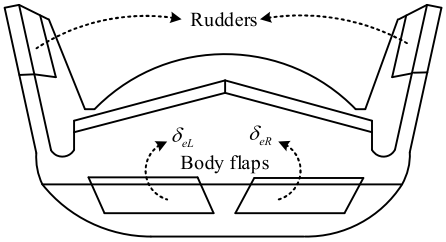

Fig. 1. Back view of X-38.

The main contributions of this article are twofold. First, accurate output tracking is achieved for an underactuated RLV by combining output redefinition and optimal bounded inversion, where output redefinition is employed to obtain stable zero dynamics and optimal bounded inversion gives the IID which are used as reference trajectories for the internal states. Compared with the existing methods in [21]–[23], the proposed method can greatly improve the output tracking accuracy for time-varying signals due to the application of IID. Second, a simple and useful anti-windup strategy is proposed by using feedback error clipping. Unlike other anti-windup strategies in [6], [7], and [26] which react when input saturation occurs, the proposed method can prevent input saturation in advance and does not require an auxiliary system. As verified by the simulation results, input saturation can be effectively avoided even when the output is required to track a drastic step command.

The remainder of this article is organized as follows. Section II introduces the underactuated RLV model. In Section III, the zero dynamics are analyzed, and output redefinition is conducted. In Section IV, optimal bounded inversion is proposed to obtain the IID. In Section V, an anti-windup robust backstepping controller is designed. Numerical simulation results are given in Section VI and conclusions are given in Section VII.

II. Underactuated RLV Model

In this section, the attitude dynamics of an underactuated RLV are given based on the X-38 model. As shown in Fig. 1, X-38 contains four aerodynamic control surfaces, including two rudders and two body flaps. Besides, it is also equipped with several RCS thrusters. In the middle phase of reentry, when the dynamic pressure is greater than 1500 Pa and the Mach number is more than 6, the RCS thrusters are no longer available because they lose efficiency in high dynamic pressure. Also, the rudders cannot be used due to the high speed, which may cause excessive thermal loads on the rudders. As a result, the available actuators are only two body flaps in this phase.

The traditional control surface deflections δ_e and δ_a (i.e., elevator and aileron) are defined by a combination of the two body flaps. The average total deflection of the two body flaps plays the role of the overall elevator, and the differential deflection of the two body flaps acts as an aileron, so that

$$\begin{aligned} \delta_e &\triangleq (\delta_{eL} + \delta_{eR})/2 \\ \delta_a &\triangleq \delta_{eL} - \delta_{eR} \end{aligned} \tag{1}$$

where δ_{eL} and δ_{eR} are the left and right deflections, respectively. The attitude of the RLV can be described by three attitude angles, α, β, and μ, which are the angles of attack, sideslip, and bank, respectively, and three angular rates, p, q, and r, which are the angular rates of roll, pitch, and yaw, respectively. Following [21] and [22], and assuming the flight path angle to be zero according to the quasi-equilibrium glide condition [27], the attitude dynamics of an underactuated RLV are written as follows:

$$\begin{aligned}
\dot{\alpha} &= -p\cos\alpha\tan\beta + q - r\sin\alpha\tan\beta + \frac{m_0 g_0\cos\mu - L}{m_0 V_0\cos\beta}\\
\dot{\beta} &= p\sin\alpha - r\cos\alpha + \frac{m_0 g_0\sin\mu - Y}{m_0 V_0}\\
\dot{\mu} &= \frac{p\cos\alpha + r\sin\alpha}{\cos\beta} + \frac{L - m_0 g_0\cos\mu}{m_0 V_0}\tan\beta\\
\dot{p} &= \frac{I_{xz}(I_x - I_y + I_z)pq + (I_y I_z - I_z^2 - I_{xz}^2)qr}{I_x I_z - I_{xz}^2} + L'_\beta\beta + L'_{\delta_a}\delta_a\\
\dot{q} &= \frac{(I_z - I_x)pr + I_{xz}(r^2 - p^2)}{I_y} + M'_\alpha\Delta\alpha + M'_{\delta_e}\Delta\delta_e\\
\dot{r} &= \frac{I_{xz}(-I_x + I_y - I_z)qr + (I_x^2 - I_x I_y + I_{xz}^2)pq}{I_x I_z - I_{xz}^2} + N'_\beta\beta\\
&\quad + N'_{\delta_a}\delta_a
\end{aligned} \tag{2}$$

where I_x, I_y, and I_z are the moments of inertia about the three body axes while I_{xz} is the cross product of inertia. m_0, V_0, and g_0 are vehicle mass, flight velocity, and gravitational acceleration, respectively. $L = L_\alpha\Delta\alpha + m_0 g_0$ and $Y = Y_\beta\beta$ represent the lift and the side force, respectively. L_α, Y_β, L'_β, L'_{δ_a}, N'_β, N'_{δ_a}, M'_α, and M'_{δ_e} are aerodynamic parameters. $\Delta\alpha = \alpha - \alpha_T$ and $\Delta\delta_e = \delta_e - \delta_{eT}$ are the deviations of α and δ_e from their trim values, where α_T is the trim value for angle of attack and δ_{eT} is the trim value for elevator deflection.

In this model, only two control inputs are available, namely, the elevator deflection δ_e and the aileron deflection δ_a. However, the system has 3 degrees of freedom, that is, the roll, pitch, and yaw. It can be observed from (2) that the pitch rate q is controlled by the elevator deflection δ_e, while the roll rate p and yaw rate r are both controlled by the aileron deflection δ_a. Therefore, the system is underactuated. Besides, the deflection of the aerodynamic control surfaces has a physical boundary limit in practice, which puts constraints for both control inputs.

The main goal of attitude control during reentry is to follow the guidance commands, including the angle of attack command α_d and the bank angle command μ_d so that the RLV can be guided from the initial entry point into a neighborhood of the landing site. Hence, we call the angle of attack α and the bank angle μ as the original outputs.

III. Zero Dynamics Analysis and Output Redefinition

In this section, the zero dynamics of the underactuated RLV model are analyzed. First, it is shown that the zero dynamics are unstable when the angle of attack and bank angle are selected as outputs. Then, a synthetic output is constructed to obtain stable zero dynamics.

Recall the underactuated RLV model (2), it is a sixth-order system. The original outputs $[\alpha, \mu]$ have the relative degree $\{2, 2\}$, indicating the existence of second-order internal dynamics which are not included in the input–output dynamics. To describe the internal dynamics, two variables are selected as the internal states. One is the sideslip angle β, and the other is a synthetic variable defined by $\eta = r - cp$, where $c = N'_{\delta_a}/L'_{\delta_a}$ is a constant. Then the internal dynamics are described by

$$\begin{aligned}
\dot{\beta} &= p\sin\alpha - (\eta + cp)\cos\alpha + \frac{m_0 g_0\sin\mu - Y}{m_0 V_0}\\
\dot{\eta} &= \left(N'_\beta - cL'_\beta\right)\beta + aq(\eta + cp) + bpq
\end{aligned} \tag{3}$$

where a and b are constants defined as follows:

$$\begin{aligned}
a &= \left[I_{xz}(-I_x + I_y - I_z) - c\left(I_y I_z - I_z^2 - I_{xz}^2\right)\right]/\left(I_x I_z - I_{xz}^2\right)\\
b &= \left[I_x^2 - I_x I_y + I_{xz}^2 - cI_{xz}(I_x - I_y + I_z)\right]/\left(I_x I_z - I_{xz}^2\right).
\end{aligned} \tag{4}$$

Remark 1: For a control system, the outputs and their derivatives up to the $(r_i - 1)$th order (r_i is the relative degree of the output y_i) are external states [28]; all state variables which cannot be fully expressed as a function of the external states are candidates for internal states. By choosing proper state variables as internal states, the input can be removed from the internal dynamics, which facilitates the stability analysis of the zero dynamics (the internal dynamics turn into zero dynamics when the outputs are identically zero). To this end, we have selected β and $\eta = r - cp$ as the internal states since both are independent of the outputs α, μ and neither contains any input in their derivatives ($\dot{r}$ and $\dot{p}$ both contain the input δ_a, and $\dot{\eta} = \dot{r} - c\dot{p}$ cancels the input).

A. Zero Dynamics of the Original Outputs

Definition 1 (Nonminimum Phase Systems [28]): Nonminimum phase systems refer to systems with unstable zero dynamics, where zero dynamics are the internal dynamics when the outputs are identically zero.

Remark 2: Zero dynamics describe the behavior of a system when the output is forced to be zero, which reflects the inherent stability of the internal states. For minimum phase systems, there are no internal states or the internal states can maintain stable by itself. While for nonminimum phase systems, the internal states cannot maintain stable by itself. Most nonlinear control methods are based on minimum-phase systems without considering the stabilization of the internal dynamics, which will lead to instability when applied to nonminimum phase systems. There are several methods available to stabilize the internal dynamics, typically, including approximate feedback linearization [29], dynamic sliding mode control [22], and output redefinition [30]. Among them, approximate feedback linearization only applies to some particular nonminimum phase systems which are caused by weak couplings. For dynamic sliding mode control, the idea is actually very similar to output redefinition, where the sliding surface can be viewed as a redefined output. Since the zero dynamics of a system are directly determined by the selected output, modifying output

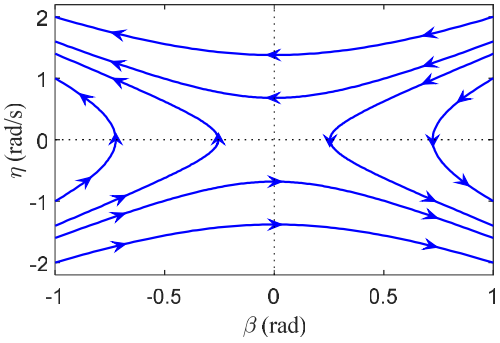

Fig. 2. Phase portrait of the original zero dynamics.

also means reassigning the zero dynamics. Output redefinition refers to redefine a new control output, typically by using a combination of the external and internal states, such that the corresponding zero dynamics are stable. Then a nonlinear controller can be designed for the new output without worrying about internal stability. The main advantage of output redefinition is that it provides a general solution to stabilize nonminimum phase systems and can be easily combined with other nonlinear control methods.

Recall the underactuated RLV model (2), for the original outputs $[\alpha, \mu]$, considering that the trim value for α is α_T, take $\Delta\alpha = \alpha - \alpha_T$ and μ as the regulated outputs. Then the zero dynamics corresponding to $[\Delta\alpha, \mu]$ are the internal dynamics constrained in the subspace $S_1 = \{\alpha \equiv \alpha_T, \mu \equiv 0\}$. Since S_1 indicates $\dot{\alpha} = 0, \dot{\mu} = 0$, it gives that

$$\begin{aligned} -p\cos\alpha_T\tan\beta + q - r\sin\alpha_T\tan\beta &= 0 \\ p\cos\alpha_T + r\sin\alpha_T &= 0. \end{aligned} \tag{5}$$

By solving (5), one obtains

$$\begin{aligned} p &= -\eta\sin\alpha_T/(\cos\alpha_T + c\sin\alpha_T) \\ q &= 0. \end{aligned} \tag{6}$$

Substituting (6) into the internal dynamics (3), the corresponding zero dynamics are obtained as

$$\begin{aligned} \dot{\beta} &= \frac{-\eta}{\cos\alpha_T + c\sin\alpha_T} - \frac{Y_\beta\beta}{m_0V_0} \\ \dot{\eta} &= \left(N'_\beta - cL'_\beta\right)\beta. \end{aligned} \tag{7}$$

To analyze the stability of the zero dynamics, the phase portrait method is applied here, which can directly show the motion of the nonlinear zero dynamics in an intuitive way. The phase portrait of the zero dynamics (7) is shown in Fig. 2. It can be observed that the origin is a typical hyperbolic equilibrium, where all states starting from the neighborhood do not converge to the origin, but go away from it, indicating that the zero dynamics are unstable. Therefore, according to Definition 1, the underactuated RLV system (2) is a nonminimum phase system with the original outputs. This prevents the direct application of typical nonlinear control methods, such as sliding mode control and dynamic inversion to the original outputs since the internal dynamics cannot maintain stable.

B. Modified Zero Dynamics Through Output Redefinition

Since the zero dynamics corresponding to the original output are unstable, it is necessary to redefine a new output to obtain stable zero dynamics. For the underactuated RLV, there are two original outputs, i.e., the angle of attack α and the bank angle μ. So there are three choices for output redefinition: 1) replace both outputs with new outputs; 2) only replace α with a new output; and 3) only replace μ with a new output. As shown in [30], the output which is modified has degraded performance when model uncertainties are considered. Therefore, it is preferred to modify only one output. So Choice 1 is not considered. For the rest two choices, we consider the case that the new output is a linear combination of the original output and the internal states (using a nonlinear combination is much more complicated in analysis and is not clear whether it can improve the performance). Therefore, the new outputs can be written as $[\alpha+b_1\beta+b_2\eta, \mu]$ for Choice 2. After trying abundant values for the coefficients b_1, b_2, it is found that the corresponding zero dynamics cannot be made stable. So Choice 2 is infeasible. For Choice 3, the new outputs are $[\alpha, \mu+\lambda_1\beta+\lambda_2\eta]$, and we find the corresponding zero dynamics can be made stable with proper coefficients λ_1 and λ_2. Therefore, the new outputs are selected as $[\alpha, \mu+\lambda_1\beta+\lambda_2\eta]$ in this article.

Denote $\upsilon = \mu+\lambda_1\beta+\lambda_2\eta$, by differentiating it one obtains

$$\begin{aligned} \dot{\upsilon} = {} & \frac{p\cos\alpha + (\eta+cp)\sin\alpha}{\cos\beta} + \frac{L - m_0g_0\cos\mu}{m_0V_0}\tan\beta \\ & + \lambda_1\left[p\sin\alpha - (\eta+cp)\cos\alpha + \frac{m_0g_0\sin\mu - Y}{m_0V_0}\right] \\ & + \lambda_2\left[\left(N'_\beta - cL'_\beta\right)\beta + aq(\eta+cp) + bpq\right]. \end{aligned} \tag{8}$$

Therefore, for $\Delta\alpha$ and the new output υ, the corresponding zero dynamics are the internal dynamics constrained in the subspace $S_2 = \{\alpha \equiv \alpha_T, \upsilon \equiv 0\}$. From $\upsilon = 0$ it can be obtained that $\mu = -\lambda_1\beta - \lambda_2\eta$. And $\dot{\alpha} = 0, \dot{\upsilon} = 0$ lead to the following equation set:

$$\begin{aligned} & \frac{m_0g_0\cos\mu - L}{m_0V_0\cos\beta} - p\cos\alpha_T\tan\beta + q \\ & \quad - (\eta+cp)\sin\alpha_T\tan\beta = 0 \\ & \frac{p\cos\alpha_T + (\eta+cp)\sin\alpha_T}{\cos\beta} + \frac{L - m_0g_0\cos\mu}{m_0V_0}\tan\beta \\ & \quad + \lambda_1\left[p\sin\alpha_T - (\eta+cp)\cos\alpha_T + \frac{m_0g_0\sin\mu - Y}{m_0V_0}\right] \\ & \quad + \lambda_2\left[\left(N'_\beta - cL'_\beta\right)\beta + aq(\eta+cp) + bpq\right] = 0 \end{aligned} \tag{9}$$

where p and q are to be solved which depend on β and η as well as the parameters λ_1 and λ_2. For brevity, the following is used to represent the solution:

$$p = p_1(\beta, \eta, \lambda_1, \lambda_2), q = q_1(\beta, \eta, \lambda_1, \lambda_2). \tag{10}$$

Substituting $\mu = -\lambda_1\beta - \lambda_2\eta$ and (10) into the internal dynamics (3) results in the following modified zero dynamics:

$$\begin{aligned} \dot{\beta} = {} & -\left[\eta + cp_1(\beta, \eta, \lambda_1, \lambda_2)\right] \\ & + \frac{m_0g_0\sin(-\lambda_1\beta - \lambda_2\eta) - Y_\beta\beta}{m_0V_0} \end{aligned}$$

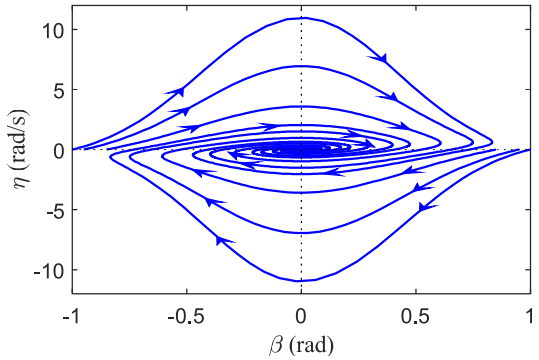

Fig. 3. Phase portrait of the modified zero dynamics.

$$\dot{\eta} = \left(N'_\beta - cL'_\beta\right)\beta + aq_1(\beta, \eta, \lambda_1, \lambda_2)\left[\eta + cp_1(\beta, \eta, \lambda_1, \lambda_2)\right] + bp_1(\beta, \eta, \lambda_1, \lambda_2)q_1(\beta, \eta, \lambda_1, \lambda_2). \tag{11}$$

It can be observed from (11) that the modified zero dynamics depend on the coefficients λ_1 and λ_2 which are the parameters to be designed in the new output. As indicated by [30], the control performance of the modified output depends on the modified zero dynamics. Therefore, the two coefficients need to be carefully selected such that: 1) the modified zero dynamics are (locally) stable and 2) the modified zero dynamics exhibit good convergent performance. To figure out the best values for λ_1 and λ_2, we treat it as a parameter optimization problem by defining the following integral square error (ISE) as the performance index:

$$J_1 = \int_0^\infty \left[\beta^2(t) + \eta^2(t)\right]dt. \tag{12}$$

Then the problem becomes to determine the coefficients λ_1 and λ_2 such that the performance index (12) is minimized subject to the zero dynamics constraint (11). To solve this optimization problem, the MATLAB function "fmincon" is applied [$\beta(0) = 1, \eta(0) = 0$ and an integral time of 100 s are applied in the programming] and the obtained optimal values are $\lambda_1 = -3.23$ and $\lambda_2 = 0.59$.

By using the obtained coefficients, the phase portrait of the modified zero dynamics (11) is shown in Fig. 3. It can be seen that the origin now becomes a stable equilibrium since all states from the neighborhood are attracted to the origin. Therefore, the modified zero dynamics are successfully stabilized with the redefined output. Hence, the controller can be designed based on the redefined output $[\alpha, \upsilon]$ so that the internal dynamics can maintain stable.

IV. IID Calculation by Optimal Bounded Inversion

In the previous section, a new control output υ is constructed which leads to stable zero dynamics. It should be noted that output redefinition is only a tool to stabilize the internal dynamics, while the real control objective is still to track the guidance commands α_d and μ_d. To achieve this goal, a desired trajectory needs to be specified for the new output υ to track such that the original outputs α and μ can track the guidance commands α_d and μ_d asymptotically. The key

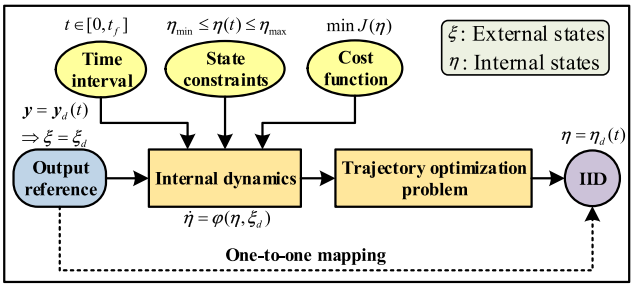

Fig. 4. IID calculation by optimal bounded inversion.

to solving this problem relies on finding a bounded solution for the internal states corresponding to the output references, which are called as IID [24].

For the given guidance commands α_d and μ_d, the IID is a bounded solution for the internal dynamics (3) constrained in the subspace $S_3 = \{\alpha \equiv \alpha_d, \mu \equiv \mu_d\}$. Taking S_3 into $\dot{\alpha}, \dot{\mu}$ gives that

$$\begin{aligned}\dot{\alpha}_d &= -p\cos\alpha_d\tan\beta + q - r\sin\alpha_d\tan\beta + \frac{m_0 g_0\cos\mu_d - L}{m_0 V_0\cos\beta}\\ \dot{\mu}_d &= \frac{p\cos\alpha_d + r\sin\alpha_d}{\cos\beta} + \frac{L - m_0 g_0\cos\mu_d}{m_0 V_0}\tan\beta.\end{aligned} \tag{13}$$

By solving (13), it follows that:

$$\begin{aligned}p &= \frac{\sin\beta(m_0 g_0\cos\mu_d - L)}{m_0 V_0(\cos\alpha_d + c\sin\alpha_d)} + \frac{\dot{\mu}_d\cos\beta - \eta\sin\alpha_d}{\cos\alpha_d + c\sin\alpha_d}\\ q &= \dot{\alpha}_d + \dot{\mu}_d\sin\beta + \frac{\cos\beta(L - m_0 g_0\cos\mu_d)}{m_0 V_0}.\end{aligned} \tag{14}$$

For brevity, denote (14) as follows:

$$p = p_d(\beta, \eta), q = q_d(\beta, \eta). \tag{15}$$

Substituting (15) into the internal dynamics (3), the corresponding internal dynamics driven by α_d and μ_d are

$$\begin{aligned}\dot{\beta} &= p_d(\beta, \eta)(\sin\alpha_d - c\cos\alpha_d) - \eta\cos\alpha_d + \left(m_0 g_0\sin\mu_d - Y_\beta\beta\right)/(m_0 V_0)\\ \dot{\eta} &= \left(N'_\beta - cL'_\beta\right)\beta + aq_d(\beta, \eta)\left[\eta + cp_d(\beta, \eta)\right] + bp_d(\beta, \eta)q_d(\beta, \eta).\end{aligned} \tag{16}$$

Therefore, the IID should be a bounded solution for the internal dynamics (16). Due to the nonminimum phase property, direct integration of (16) will lead to an unbounded solution and thus cannot be used to get the IID. Here, a method called optimal bounded inversion [25] is used to get the IID, whose main idea is to transfer the IID calculation into a trajectory optimization problem as shown in Fig. 4.

For the underactuated RLV studied in this article, the optimal bounded inversion problem is defined as follows.

Optimal Bounded Inversion Problem: Giving the guidance commands $\alpha_d(t)$ and $\mu_d(t)$ in the time interval $t \in [0, t_f]$, determine the trajectory $\beta(t)$ and $\eta(t)$ that minimizes the cost function

$$J = \int_0^{t_f}\left(\beta^2 + \eta^2\right)d\tau \tag{17}$$

subject to the dynamic constraints (16) and the state constraints

$$\beta_m \le \beta \le \beta_M, \;\; \eta_m \le \eta \le \eta_M \tag{18}$$

where $[\beta_m, \beta_M]$ and $[\eta_m, \eta_M]$ are the desired boundaries for β and η, respectively.

By setting the above trajectory optimization problem, the boundedness of the IID can be guaranteed by the state constraints (18). Besides, the cost function (17) aims to minimize the overall quadratic cost of the internal states, thus can keep the internal states as small as possible. The optimal bounded inversion problem defined above can be easily solved by using the powerful optimization software GPOPS-II [31], which guarantees high efficiency as well as high accuracy for the IID calculation.

Remark 3: It is not our goal to propose any new methods in solving the above trajectory optimization problem, while the idea itself is new to treat IID calculation as a trajectory optimization problem. So far there are three existing methods for IID calculation, including output regulation [32], [33], stable system center [34], [35], and stable inversion [36], [37]. The proposed optimal bounded inversion method has some advantages over the existing ones. First, compared with output regulation and stable system center, the proposed method does not rely on the assumption of an exosystem to generate the output reference and thus can be applied to arbitrary output reference. Second, compared with stable inversion, the proposed method is much easier to understand and to implement. Stable inversion involves a Picard-like iteration process that puts barriers for its implementation, while in the proposed method, the only thing we need to do is to get the internal dynamics and construct the trajectory optimization problem, which can then be solved by the existing software.

Denoting the resulted IID as β_d and η_d, they can be used as the reference trajectories for the internal states. That is, for the new output $\upsilon = \mu + \lambda_1\beta + \lambda_2\eta$, the desired trajectory can be designed as $\upsilon_d = \mu_d + \lambda_1\beta_d + \lambda_2\eta_d$ so that the original output μ can track μ_d when υ tracks υ_d according to [24].

V. Controller Design

The overall control architecture is shown in Fig. 5. As output redefinition has been accomplished in Section III and the desired trajectory υ_d has been specified in Section IV, this section focuses on designing a robust backstepping controller such that α, υ track the references α_d and υ_d. The input constraints are considered here, and an anti-windup strategy is proposed.

A. Control-Oriented Model

To apply backstepping control, it is necessary to write the model in a strict-feedback form. For convenience, denote $\mathbf{y} = [\alpha, \upsilon]^T$, $\boldsymbol{\omega} = [p, q]^T$, and $\mathbf{u} = [\delta_e, \delta_a]^T$, then the underactuated RLV model can be transformed into the following control-oriented model:

$$\begin{aligned} \dot{\mathbf{y}} &= \mathbf{F}_1 + \mathbf{G}_1\boldsymbol{\omega} + \mathbf{d}_1 \\ \dot{\boldsymbol{\omega}} &= \mathbf{F}_2 + \mathbf{G}_2\mathbf{u} + \mathbf{d}_2 \end{aligned} \tag{19}$$

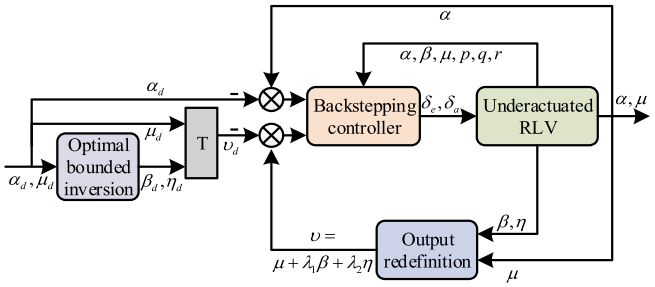

Fig. 5. Overall control architecture.

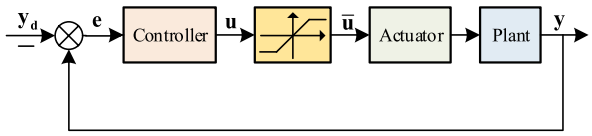

Fig. 6. Control structure with input clipping.

where $\mathbf{d}_1$ and $\mathbf{d}_2$ are lumped disturbances caused by model uncertainties, and $\mathbf{F}_1$, $\mathbf{F}_2$, $\mathbf{G}_1$, and $\mathbf{G}_2$ are defined as follows:

$$\mathbf{F}_1 = \begin{bmatrix} -\eta \sin\alpha \tan\beta + \frac{m_0 g_0 \cos\mu - L}{m_0 V_0 \cos\beta} \\ f_{12} \end{bmatrix}$$

$$\begin{aligned} f_{12} = {} & \frac{(L - m_0 g_0 \cos\mu)\tan\beta + \lambda_1(m_0 g_0 \sin\mu - Y)}{m_0 V_0} \\ & + \eta \sin\alpha / \cos\beta - \lambda_1 \eta \cos\alpha + \lambda_2 \dot{\eta} \end{aligned} \tag{20}$$

$$\mathbf{G}_1 = \begin{bmatrix} -\cos\alpha\tan\beta - c\sin\alpha\tan\beta & 1 \\ \frac{\cos\alpha + c\sin\alpha}{\cos\beta} + \lambda_1(\sin\alpha - c\cos\alpha) & 0 \end{bmatrix} \tag{21}$$

$$\mathbf{F}_2 = \begin{bmatrix} \frac{I_{xz}(I_x - I_y + I_z)pq + (I_y I_z - I_z^2 - I_{xz}^2)qr}{I_x I_z - I_{xz}^2} + L'_\beta \beta \\ \frac{(I_z - I_x)pr + I_{xz}(r^2 - p^2)}{I_y} + M'_\alpha \Delta\alpha - M'_{\delta_e}\delta_{eT} \end{bmatrix} \tag{22}$$

$$\mathbf{G}_2 = \begin{bmatrix} 0 & L'_{\delta_a} \\ M'_{\delta_e} & 0 \end{bmatrix}. \tag{23}$$

It should be noted that the control-oriented model (19) has a similar form but with reduced order compared to the original model (2). The internal dynamics are not listed in (19) since they can maintain stable by itself, and we only need to consider tracking control for the new output in the next. Thanks to output redefinition, the original control problem of an underactuated system is transferred into an equivalent control problem of a fully actuated system (19), where various nonlinear control methods can be readily applied.

B. Anti-Windup Robust Backstepping Controller Design

Fig. 6 shows the control structure with input clipping. The key point of input clipping is to limit the magnitude of the calculated input compulsively by placing a magnitude clipper just after the controller, so that the input command sent to the actuator keeps within the input constraints. However, when using this control structure, it may cause input saturation, which can lead to instability.

As an improvement, the magnitude clipper can be moved to the position just before the controller, which results in a new control structure with feedback error clipping as shown in Fig. 7. Considering that input saturation is usually caused by

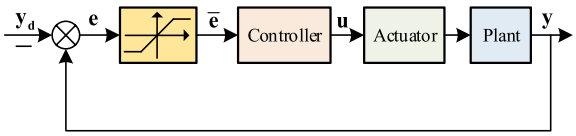

Fig. 7. Control structure with feedback error clipping.

a large instantaneous tracking error which generates a large input for correction, by using the clipped feedback error in the controller, a relatively small input is generated so that the input saturation problem can be avoided.

In Fig. 7, $\bar{\mathbf{e}} = [\bar{e}_1, \bar{e}_2]^T$ is the clipped feedback error, and the magnitude clipper is designed as follows:

$$\bar{e}_i = \begin{cases} \varepsilon_i, & \text{if } e_i > \varepsilon_i \\ e_i, & \text{if } |e_i| \le \varepsilon_i \\ -\varepsilon_i, & \text{if } e_i < -\varepsilon_i \end{cases} \tag{24}$$

where ε_i $(i = 1, 2)$ is a positive constant that limits the upper bound of the feedback error. The function of feedback error clipping can also be interpreted in another way, that is, it is equivalent to modifying the output command as follows:

$$\bar{y}_{\mathrm{id}} = \begin{cases} y_i - \varepsilon_i, & \text{if } e_i > \varepsilon_i \\ y_{\mathrm{id}}, & \text{if } |e_i| \le \varepsilon_i \\ y_i + \varepsilon_i, & \text{if } e_i < -\varepsilon_i \end{cases} \tag{25}$$

where $y_i (i = 1, 2)$ represents α, υ, respectively, $y_{\mathrm{id}} (i = 1, 2)$ represents α_d and υ_d, respectively, and $\bar{y}_{\mathrm{id}} (i = 1, 2)$ is the clipped output command. It is easy to verify that the clipped feedback error can be viewed as the error between the output and the clipped command, that is, $\bar{e}_i = y_i - \bar{y}_{\mathrm{id}}$. Therefore, an intuitional interpretation of (25) is: feedback error clipping modifies the output command to make it closer to the current output value. This explains why feedback error clipping can avoid input saturation.

Remark 4: The threshold ε_i is important in preventing input saturation. Since it is hard to determine its best value mathematically, tuning it through simulation is a good option. If ε_i is large, say, exceeds the possible bound of the maximum error, then it is equal to turn off the feedback error clipper and input saturation may occur. So generally speaking, ε_i should be small to prevent input saturation. However, the tracking error will converge slowly if ε_i is too small. So the suggested principle of tuning ε_i is to consider the maximum initial tracking error case, and start with a small ε_i, then increase it bit by bit until the input is close to saturation.

For the RLV system (19), the original command for $\mathbf{y}$ is $\mathbf{y_d} = [\alpha_d, \upsilon_d]^T$. Define the clipped feedback error $\bar{\mathbf{e}} = \mathbf{y} - \bar{\mathbf{y}}_\mathbf{d}$, where $\bar{\mathbf{y}}_\mathbf{d} = [\bar{y}_{1d}, \bar{y}_{2d}]^T$ is the clipped output command defined by (25). Then $\dot{\bar{\mathbf{e}}} = \dot{\mathbf{y}} - \dot{\bar{\mathbf{y}}}_\mathbf{d} = \dot{\mathbf{y}} - \dot{\mathbf{y}}_\mathbf{d} + (\dot{\mathbf{y}}_\mathbf{d} - \dot{\bar{\mathbf{y}}}_\mathbf{d})$ can be written as follows:

$$\dot{\bar{\mathbf{e}}} = \mathbf{F}_1 - \dot{\mathbf{y}}_\mathbf{d} + \mathbf{G}_1\boldsymbol{\omega} + \mathbf{d}_1 \tag{26}$$

where $\dot{\mathbf{y}}_\mathbf{d} - \dot{\bar{\mathbf{y}}}_\mathbf{d}$ is incorporated into the lumped disturbance $\mathbf{d}_1$. Assume that $\|\mathbf{d}_1\| \le D_1$ where D_1 is a constant. Consider the angular rate ω as a virtual control and the desired angular rate is designed as follows (it is assumed that $\bar{\mathbf{e}}/\|\bar{\mathbf{e}}\| = \mathbf{0}$ for $\bar{\mathbf{e}} = \mathbf{0}$):

$$\boldsymbol{\omega}_\mathbf{d} = \mathbf{G}_1^{-1}\left(-\mathbf{F}_1 + \dot{\mathbf{y}}_\mathbf{d} - k_1\bar{\mathbf{e}} - \frac{\hat{D}_1\bar{\mathbf{e}}}{\|\bar{\mathbf{e}}\|}\right) \tag{27}$$

where $k_1 > 0$. The last item on the right side is a robust item with $\hat{D}_1$ be the estimation of the disturbance upper bound.

Remark 5: For the given parameters $c = -0.0494$ (model parameter), $\lambda_1 = -3.23$ (controller parameter), and the admissible flight range $\alpha \in [10, 50]$ deg, $\beta \approx 0$, it can be verified that $0.135 \le \det(\mathbf{G}_1) \le 3.384$, which indicates that $\mathbf{G}_1$ is invertible.

Define $\tilde{\boldsymbol{\omega}} = \boldsymbol{\omega} - \boldsymbol{\omega}_\mathbf{d}$ as the tracking error of the angular rate. Substituting (27) into (26) results in

$$\dot{\bar{\mathbf{e}}} = \mathbf{G}_1\tilde{\boldsymbol{\omega}} - k_1\bar{\mathbf{e}} - \frac{\hat{D}_1\bar{\mathbf{e}}}{\|\bar{\mathbf{e}}\|} + \mathbf{d}_1. \tag{28}$$

Now consider the angular rate error dynamics

$$\dot{\tilde{\boldsymbol{\omega}}} = \mathbf{F}_2 + \mathbf{G}_2\mathbf{u} + \mathbf{d}_2 \tag{29}$$

where $-\dot{\boldsymbol{\omega}}_\mathbf{d}$ is incorporated into the lumped disturbance $\mathbf{d}_2$.

Assuming $\|\mathbf{d}_2\| \le D_2$ where D_2 is a constant, the control input is then designed as follows (it is assumed that $\tilde{\boldsymbol{\omega}}/\|\tilde{\boldsymbol{\omega}}\| = \mathbf{0}$ for $\tilde{\boldsymbol{\omega}} = \mathbf{0}$):

$$\mathbf{u} = \mathbf{G}_2^{-1}\left(-\mathbf{F}_2 - k_2\tilde{\boldsymbol{\omega}} - \mathbf{G}_1^T\bar{\mathbf{e}} - \frac{\hat{D}_2\tilde{\boldsymbol{\omega}}}{\|\tilde{\boldsymbol{\omega}}\|}\right) \tag{30}$$

where $k_2 > 0$ and $\hat{D}_2$ is the estimation of the upper bound for the disturbance.

Substituting (30) into (29) yields

$$\dot{\tilde{\boldsymbol{\omega}}} = -k_2\tilde{\boldsymbol{\omega}} - \mathbf{G}_1^T\bar{\mathbf{e}} - \frac{\hat{D}_2\tilde{\boldsymbol{\omega}}}{\|\tilde{\boldsymbol{\omega}}\|} + \mathbf{d}_2. \tag{31}$$

The adaptive law is designed as follows:

$$\begin{aligned} \dot{\hat{D}}_1 &= \begin{cases} c_1\|\bar{\mathbf{e}}\|, & \text{if } \|(\bar{\mathbf{e}}, \tilde{\boldsymbol{\omega}})\| > \delta \\ 0, & \text{if } \|(\bar{\mathbf{e}}, \tilde{\boldsymbol{\omega}})\| \le \delta \end{cases} \\ \dot{\hat{D}}_2 &= \begin{cases} c_2\|\tilde{\boldsymbol{\omega}}\|, & \text{if } \|(\bar{\mathbf{e}}, \tilde{\boldsymbol{\omega}})\| > \delta \\ 0, & \text{if } \|(\bar{\mathbf{e}}, \tilde{\boldsymbol{\omega}})\| \le \delta \end{cases} \end{aligned} \tag{32}$$

where $c_1, c_2 > 0$, and $\delta > 0$ is a threshold to prevent that $\hat{D}_1$ and $\hat{D}_2$ from increasing endlessly.

Theorem 1: Consider the control-oriented model (19), when the controller (30) along with the adaptive law (32) is applied, the output tracking error $\mathbf{e} = \mathbf{y} - \mathbf{y_d}$ will converge to a small region around zero.

Proof: Select the candidate Lyapunov function as $V = (1/2)\bar{\mathbf{e}}^T\bar{\mathbf{e}} + (1/2)\tilde{\boldsymbol{\omega}}^T\tilde{\boldsymbol{\omega}} + (1/2c_1)\tilde{D}_1^2 + (1/2c_2)\tilde{D}_2^2$. When $\|(\bar{\mathbf{e}}, \tilde{\boldsymbol{\omega}})\| > \delta$, the derivative of V is given by

$$\begin{aligned} \dot{V} &= \bar{\mathbf{e}}^T\left(\mathbf{G}_1\tilde{\boldsymbol{\omega}} - k_1\bar{\mathbf{e}} - \frac{\hat{D}_1\bar{\mathbf{e}}}{\|\bar{\mathbf{e}}\|} + d_1\right) - \tilde{D}_1\|\bar{\mathbf{e}}\| - \tilde{D}_2\|\tilde{\boldsymbol{\omega}}\| \\ &\quad + \tilde{\boldsymbol{\omega}}^T\left(-k_2\tilde{\boldsymbol{\omega}} - \boldsymbol{G}_1^T\bar{\mathbf{e}} - \frac{\hat{D}_2\tilde{\boldsymbol{\omega}}}{\|\tilde{\boldsymbol{\omega}}\|} + \mathbf{d}_2\right) \\ &\le -k_1\|\bar{\mathbf{e}}\|^2 - \hat{D}_1\|\bar{\mathbf{e}}\| + \|\bar{\mathbf{e}}\|\|\mathbf{d}_1\| - k_2\|\tilde{\boldsymbol{\omega}}\|^2 - \hat{D}_2\|\tilde{\boldsymbol{\omega}}\| \\ &\quad + \|\tilde{\boldsymbol{\omega}}\|\|\mathbf{d}_2\| - \tilde{D}_1\|\bar{\mathbf{e}}\| - \tilde{D}_2\|\tilde{\boldsymbol{\omega}}\| \\ &= -k_1\|\bar{\mathbf{e}}\|^2 - k_2\|\tilde{\boldsymbol{\omega}}\|^2 + \|\bar{\mathbf{e}}\|(\|\mathbf{d}_1\| - D_1) \end{aligned}$$

$$+ \|\tilde{\boldsymbol{\omega}}\|(\|\mathbf{d}_2\| - D_2)$$
$$\leq -k_1\|\bar{\mathbf{e}}\|^2 - k_2\|\tilde{\boldsymbol{\omega}}\|^2 \leq 0. \quad (33)$$

Therefore, the closed-loop system is stable and the system signal will converge to the attraction basin $\|(\bar{\mathbf{e}}, \tilde{\boldsymbol{\omega}})\| \leq \delta$. By choosing proper parameters, the clipped feedback error $\bar{\mathbf{e}}$ will converge to a small region around zero. The convergence of the actual tracking error $\mathbf{e} = \mathbf{y} - \mathbf{y_d} = [e_1, e_2]^T$ is composed of two phases as follows.

Phase 1: When $e_i > \varepsilon_i$ (or $e_i < -\varepsilon_i$), the modified output reference is $\bar{y}_{\mathrm{id}} = y_i - \varepsilon_i$ (or $\bar{y}_{\mathrm{id}} = y_i + \varepsilon_i$), then y_i tends to converge to $\bar{y}_{\mathrm{id}}$ but will never reach since the command $\bar{y}_{\mathrm{id}} = y_i - \varepsilon_i$ keeps declining (or rising). As a result, the output will keep decreasing (or increasing) until $e_i = \varepsilon_i$ (or $e_i = -\varepsilon_i$). After that, Phase 1 ends and the system goes to Phase 2.

Phase 2: When $|e_i| \leq \varepsilon_i$, then $e_i = \bar{e}_i$, and e_i will converge to a small region around zero. This completes the proof. ■

VI. Numerical Simulations

In the simulation, the control input constraints are assumed to be $\delta_e \in [0, 50]$ deg and $\delta_a \in [-25, 25]$ deg according to [20]. The aerodynamic parameters are $L'_\beta = -25.1$, $L'_{\delta_a} = -10.6$, $N'_\beta = -1.53$, $N'_{\delta_a} = 0.53$, $L_\alpha = 1200$, $Y_\beta = 2.5$, $M'_\alpha = 10$, and $M'_{\delta_e} = 15$. The moments of inertia are $I_x = 203.4$, $I_y = 1356$, $I_z = 1627$, $I_{xz} = 27.1$ slug·ft^2. Other model parameters are $m_0 = 68.5$ slug, $V_0 = 17192$ ft/s, $g_0 = 32.2$ ft/s^2, $\alpha_T = 0.66$ rad, $\delta_{eT} = 0.17$ rad. The controller parameters are $\lambda_1 = -3.23$, $\lambda_2 = 0.59$, $k_1 = 10$, $k_2 = 5$, $c_1 = 10$, $c_2 = 10$, $\delta = 0.02$, $\varepsilon_1 = 0.0087$rad$(0.5\,\mathrm{deg})$, and $\varepsilon_2 = 0.0175$rad$(1\,\mathrm{deg})$.

The simulations are performed in MATLAB R2017a. First, step command tracking is investigated to verify the anti-windup capability of the proposed controller. Then, a trajectory tracking task is performed to further verify the effectiveness of the proposed controller in handling the nonminimum phase problem, control input constraints, and model uncertainties. The initial conditions are set to $\beta(0) = 0$, $p(0) = 0$, $q(0) = 0$, and $r(0) = 0$ for all simulations while the outputs $\alpha(0)$, $\mu(0)$ depend on different cases which are shown later.

A. Step Command Tracking

Step command tracking is used to test the capability of the controller in tackling control input constraints since the system is most likely to encounter input saturation with a large initial error. For comparison, simulations are first done by using input clipping. Fig. 8 shows the simulation results when the bank angle is required to move from 20 deg to 0 deg. In this case, instability is observed for the two outputs which do not converge but go to large values, and input chattering is observed for both control inputs. This illustrates that the input clipping method has failed to handle input constraints.

With the proposed anti-windup strategy by using feedback error clipping, the problem above can be avoided. Fig. 9 shows the results of 100 Monte Carlo runs by using feedback error clipping, where the initial values of the angle of attack and bank angle are uniformly distributed in the range $\alpha(0) \in [10, 40]\,\mathrm{deg}$, $\mu(0) \in [-30, 30]\,\mathrm{deg}$ and are required to track the step commands $\alpha_d = 25\,\mathrm{deg}$, $\mu_d = 0$. It can be observed

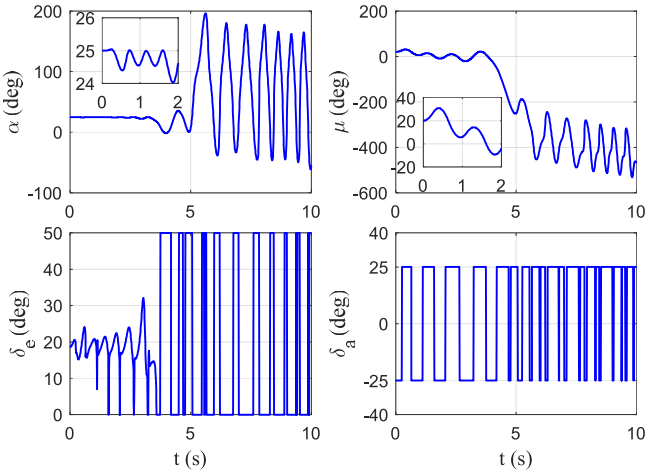

Fig. 8. Step command tracking for the angle of attack with input clipping.

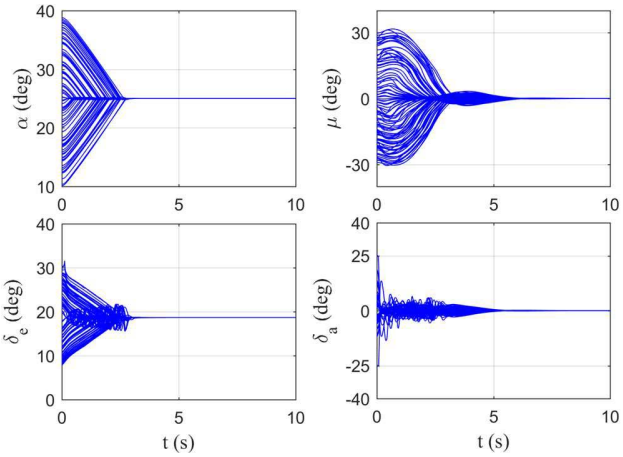

Fig. 9. Monte Carlo simulation results for step command tracking with feedback error clipping.

that both outputs converge to the desired values quickly and the two inputs keep within the constraint range $\delta_e \in [0, 50]$ deg, $\delta_a \in [-25, 25]$ deg, which demonstrates the excellent performance of the proposed anti-windup strategy.

Fig. 10 shows the step command tracking details of the redefined control output $\mathbf{y} = [\alpha, \upsilon]^T$ when using feedback error clipping method. It can be observed that the clipped command remains close to the output value, which is the key to preventing the input from saturation. Both outputs follow the two-phase convergence rule described in the end of Section V, that is, the output first goes toward the predefined clipped error threshold (0.5 deg for α and 1 deg for υ), and once get into, it will not go out but converge to the desired command.

Fig. 11 shows a comparison of the simulation results between constrained adaptive backstepping [6], [26] and the proposed anti-windup method. It can be observed from the top part that the outputs in constrained adaptive backstepping converge faster than that of the proposed method. However, it is at the cost of input chattering as shown in the bottom part, where the inputs in constrained adaptive backstepping change drastically between the maximum and minimum values in the beginning (this is also observed in [26]). On the contrary, the

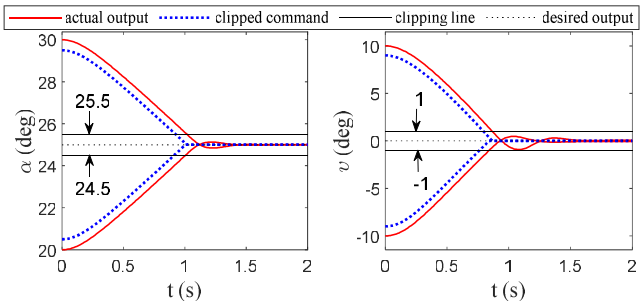

Fig. 10. Step command tracking details with feedback error clipping.

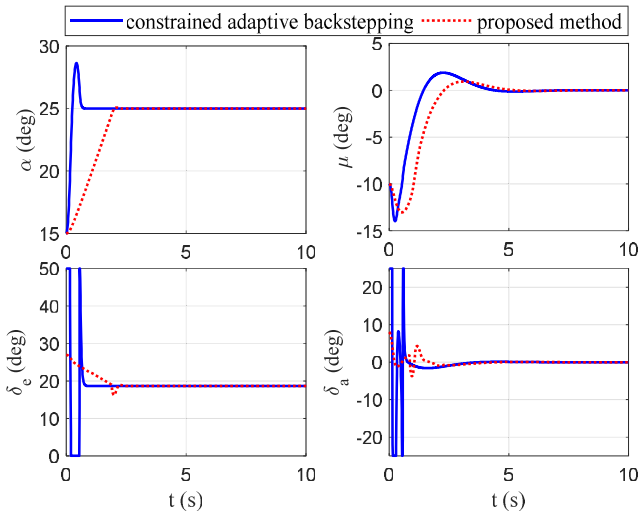

Fig. 11. Comparison between constrained adaptive backstepping and the proposed anti-windup method.

inputs obtained by the proposed method change much more smoothly and never reach the constrained boundaries. This verifies the advantage of the proposed anti-windup method, that is, it can avoid input saturation and obtain smooth input, while other methods [6], [7], [26] take action when input saturation occurs and often induce input chattering.

B. Trajectory Tracking

In practice, the guidance commands are time-varying signals. To verify the trajectory tracking performance of the proposed controller in the existence of the nonminimum phase problem as well as control input constraints and model uncertainties, a trajectory tracking task is simulated. The reference commands for the angle of attack and bank angle are taken from [21]. The corresponding IID are obtained by the optimal bounded inversion method and are incorporated into the controller. The simulation results for the nominal model are shown in Figs. 12–15 and Monte Carlo simulation results with model dispersion are given in Fig. 16.

Fig. 12 shows the actual and commanded angle of attack and bank angle and their tracking errors. It can be seen that the actual and commanded trajectories nearly coincide with each other for both angles and the tracking errors are very small. Therefore, the accurate tracking objective is well achieved.

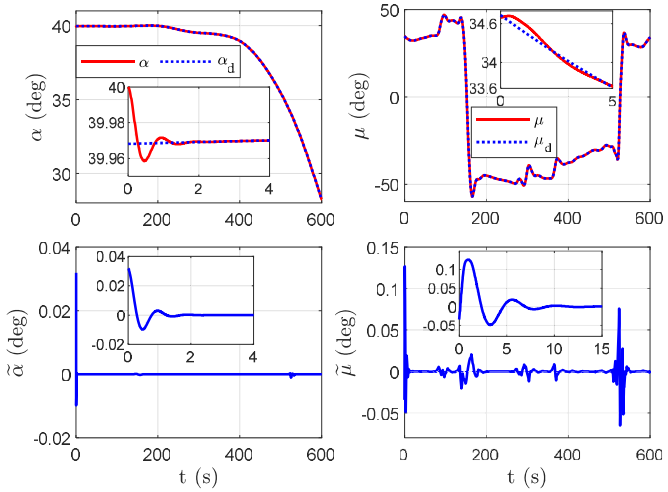

Fig. 12. Curves of the angle of attack and bank angle.

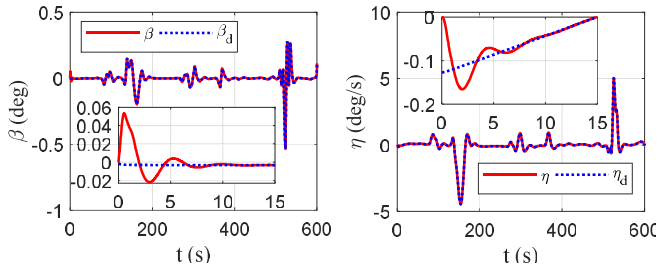

Fig. 13. Curves of the internal states.

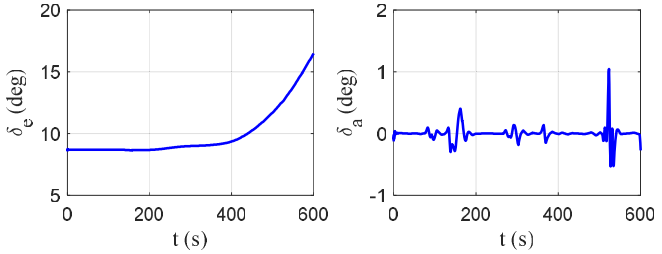

Fig. 14. Curves of the control inputs.

Fig. 13 shows the curves of the internal states. It can be observed that both internal states converge to the IID and are bounded in a feasible range. This verifies the effectiveness of the proposed method in guaranteeing the stability of the internal states.

Fig. 14 shows the curves of the control inputs, where no saturation is observed for both control inputs.

Fig. 15 presents a comparison of the tracking errors when IID are applied (β_d and η_d obtained by optimal bounded inversion) and not applied (β_d and η_d set to zero). It can be observed that the results for the angle of attack are nearly the same in both cases. However, for the bank angle, the tracking performance has a significant improvement when the IID are applied. This is easy to understand since the bank angle is replaced by a redefined output during controller design. The tracking controller directly forces that $\alpha \to \alpha_d, \upsilon \to \upsilon_d$, where $\mu \to \mu_d$ is achieved by specifying υ_d with the obtained IID. Therefore, it verifies that the application of IID is very

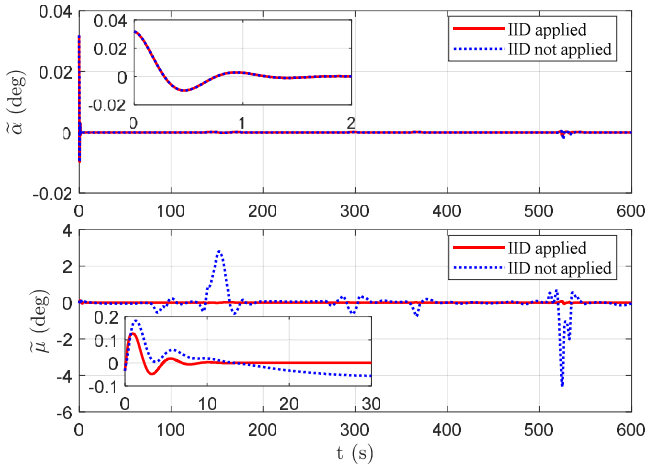

Fig. 15. Tracking errors when IID are applied/not applied.

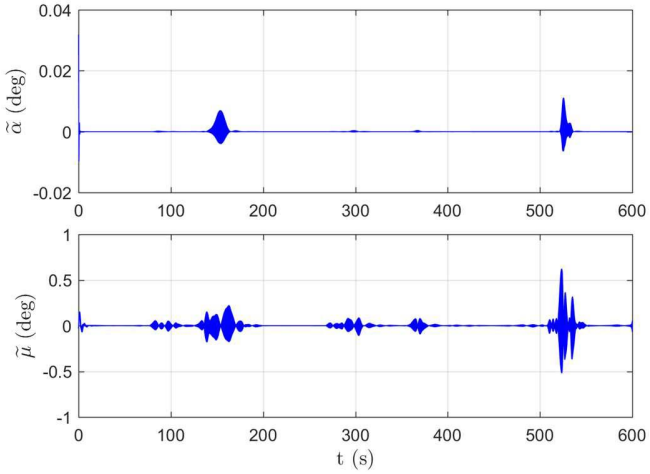

Fig. 16. Monte Carlo simulation results with model uncertainties.

important to achieve accurate output tracking for nonminimum phase systems.

Fig. 16 shows the results of 1000 Monte Carlo runs considering model uncertainties, where the inertia parameters in the model are assumed to have a random deviation within $\pm 30\%$ from their nominal values. From Fig. 16 it can be observed that both output tracking errors remain in a small region around zero, indicating that the proposed controller has good robustness against model uncertainties.

VII. Conclusion

RLVs may experience underactuation during the middle phase of reentry, which can lead to failure of the traditional methods that are designed for a fully actuated RLV. This article considers the realistic control issues for an underactuated RLV involving both nonminimum phase problem and control input constraints. An integrated controller based on the backstepping control framework is developed. To handle the nonminimum phase problem, output redefinition is employed to obtain stable zero dynamics and optimal bounded inversion is proposed to obtain the IID as reference trajectories for the internal states. The proposed method achieves accurate output tracking and ensures the stability of the internal states as well. To handle input constraints, a simple and useful anti-windup strategy is proposed by using feedback error clipping, which is shown to be very effective at avoiding input saturation even when tracking a drastic step command. In particular, the overall approach shown here provides a practical solution to achieving RLV reentry attitude tracking control under realistic conditions, which has been demonstrated through several simulation trials. The proposed control architecture may also be applied to other underactuated systems with input constraints.

References

[1] J. E. Stott and Y. B. Shtessel, "Launch vehicle attitude control using sliding mode control and observation techniques," *J. Franklin Inst.*, vol. 349, no. 2, pp. 397–412, 2012.

[2] B. Tian, L. Yin, and H. Wang, "Finite-time reentry attitude control based on adaptive multivariable disturbance compensation," *IEEE Trans. Ind. Electron.*, vol. 62, no. 9, pp. 5889–5898, Sep. 2015.

[3] Z. Guo, J. Chang, J. Guo, and J. Zhou, "Adaptive twisting sliding mode algorithm for hypersonic reentry vehicle attitude control based on finite-time observer," *ISA Trans.*, vol. 77, pp. 20–29, 2018.

[4] C. E. Hall and Y. B. Shtessel, "Sliding mode disturbance observer-based control for a reusable launch vehicle," *J. Guid. Control Dyn.*, vol. 29, no. 6, pp. 1315–1328, 2006.

[5] J. Sun, J. Yi, Z. Pu, and X. Tan, "Fixed-time sliding mode disturbance observer-based nonsmooth backstepping control for hypersonic vehicles," *IEEE Trans. Syst., Man, Cybern., Syst.*, early access, Jul. 2, 2018, doi: 10.1109/TSMC.2018.2847706.

[6] F. Wang, C. Hua, and Q. Zong, "Attitude control of reusable launch vehicle in reentry phase with input constraint via robust adaptive backstepping control," *Int. J. Adapt. Control Signal Process.*, vol. 29, no. 10, pp. 1308–1327, 2015.

[7] G. Ma, C. Chen, Y. Lyu, and Y. Guo, "Adaptive backstepping-based neural network control for hypersonic reentry vehicle with input constraints," *IEEE Access*, vol. 6, pp. 1954–1966, 2017.

[8] H. Liu, W. Bao, H. Li, and Y. Liao, "Multivariable disturbance observer-based fuzzy fast terminal sliding mode attitude control for a hypersonic vehicle," *J. Aerosp. Eng.*, vol. 32, no. 2, 2018, Art. no. 04018152.

[9] B. Xu, X. Wang, and Z. Shi, "Robust adaptive neural control of nonminimum phase hypersonic vehicle model," *IEEE Trans. Syst., Man, Cybern., Syst.*, early access, Feb. 15, 2019, doi: 10.1109/TSMC.2019.2894916.

[10] H. Sun, L. Hou, G. Zong, and X. Yu, "Adaptive decentralized neural network tracking control for uncertain interconnected nonlinear systems with input quantization and time delay," *IEEE Trans. Neural Netw. Learn. Syst.*, vol. 31, no. 4, pp. 1401–1409, Apr. 2020.

[11] J. Liu, H. An, Y. Gao, C. Wang, and L. Wu, "Adaptive control of hypersonic flight vehicles with limited angle-of-attack," *IEEE/ASME Trans. Mechatronics*, vol. 23, no. 2, pp. 883–894, Apr. 2018.

[12] Y. Gao, J. Liu, Z. Wang, and L. Wu, "Interval type-2 FNN-based quantized tracking control for hypersonic flight vehicles with prescribed performance," *IEEE Trans. Syst., Man, Cybern., Syst.*, early access, May 1, 2019, doi: 10.1109/TSMC.2019.2911726.

[13] X. Shao and H. Wang, "Back-stepping robust trajectory linearization control for hypersonic reentry vehicle via novel tracking differentiator," *J. Franklin Inst.*, vol. 353, no. 9, pp. 1957–1984, 2016.

[14] Z. Guo, J. Zhou, J. Guo, J. Cieslak, and J. Chang, "Coupling-characterization-based robust attitude control scheme for hypersonic vehicles," *IEEE Trans. Ind. Electron.*, vol. 64, no. 8, pp. 6350–6361, Aug. 2017.

[15] G. Zong, W. Qi, and H. R. Karimi, "L_1 control of positive semi-Markov jump systems with state delay," *IEEE Trans. Syst., Man, Cybern., Syst.*, early access, Mar. 24, 2020, doi: 10.1109/TSMC.2020.2980034.

[16] D. Xu, B. Jiang, and P. Shi, "Robust NSV fault-tolerant control system design against actuator faults and control surface damage under actuator dynamics," *IEEE Trans. Ind. Electron.*, vol. 62, no. 9, pp. 5919–5928, Sep. 2015.

[17] H. An, J. Liu, C. Wang, and L. Wu, "Approximate back-stepping fault-tolerant control of the flexible air-breathing hypersonic vehicle," *IEEE/ASME Trans. Mechatronics*, vol. 21, no. 3, pp. 1680–1691, Jun. 2016.

[18] L. Ma, N. Xu, X. Zhao, G. Zong, and X. Huo, "Small-gain technique-based adaptive neural output-feedback fault-tolerant control of switched nonlinear systems with unmodeled dynamics," *IEEE Trans. Syst., Man, Cybern., Syst.*, early access, Feb. 6, 2020, doi: 10.1109/TSMC.2020.2964822.
[19] R. R. Da Costa, Q. P. Chu, and J. A. Mulder, "Reentry flight controller design using nonlinear dynamic inversion," *J. Spacecr. Rockets*, vol. 40, no. 1, pp. 64–71, 2003.
[20] W. R. Van Soest, Q. P. Chu, and J. A. Mulder, "Combined feedback linearization and constrained model predictive control for entry flight," *J. Guid. Control Dyn.*, vol. 29, no. 2, pp. 427–434, 2006.
[21] E. M. Wallner and K. H. Well, "Attitude control of a reentry vehicle with internal dynamics," *J. Guid. Control Dyn.*, vol. 26, no. 6, pp. 846–854, 2003.
[22] Z. Wang, W. Bao, and H. Li, "Second-order dynamic sliding-mode control for nonminimum phase underactuated hypersonic vehicles," *IEEE Trans. Ind. Electron.*, vol. 64, no. 4, pp. 3105–3112, Apr. 2017.
[23] W. Nie, H. Li, and R. Zhang, "Observer-based attitude controller for lifting re-entry vehicle with non-minimum phase property," *Int. J. Adv. Robot. Syst.*, vol. 14, no. 3, 2017, Art. no. 1729881417703953.
[24] S. Gopalswamy and J. K. Hedrick, "Tracking nonlinear non-minimum phase systems using sliding control," *Int. J. Control*, vol. 57, no. 5, pp. 1141–1158, 1993.
[25] L. Ye, Q. Zong, and B. Tian, "Output tracking of uncertain nonminimum phase systems by experience replay," *IEEE Trans. Syst., Man, Cybern., Syst.*, early access, Jun. 13, 2019, doi: 10.1109/TSMC.2019.2919012.
[26] M. Chen, S. S. Ge, and B. Ren, "Adaptive tracking control of uncertain MIMO nonlinear systems with input constraints," *Automatica*, vol. 47, no. 3, pp. 452–465, 2011.
[27] Z. Shen and P. Lu, "Onboard generation of three-dimensional constrained entry trajectories," *J. Guid. Control Dyn.*, vol. 26, no. 1, pp. 111–121, 2003.
[28] A. Isidori, *Nonlinear Control Systems*. London, U.K.: Springer, 2013.
[29] J. T. Parker, A. Serrani, S. Yurkovich, M. A. Bolender, and D. B. Doman, "Control-oriented modeling of an air-breathing hypersonic vehicle," *J. Guid. Control Dyn.*, vol. 30, no. 3, pp. 856–869, 2007.
[30] L. Ye, Q. Zong, J. L. Crassidis, and B. Tian, "Output-redefinition-based dynamic inversion control for a nonminimum phase hypersonic vehicle," *IEEE Trans. Ind. Electron.*, vol. 65, no. 4, pp. 3447–3457, Apr. 2018.
[31] M. A. Patterson and A. V. Rao, "GPOPS-II: A MATLAB software for solving multiple-phase optimal control problems using hp-adaptive Gaussian quadrature collocation methods and sparse nonlinear programming," *ACM Trans. Math. Softw.*, vol. 41, no. 1, pp. 1–37, 2014.
[32] A. Isidori and C. I. Byrnes, "Output regulation of nonlinear systems," *IEEE Trans. Autom. Control*, vol. 35, no. 2, pp. 131–140, Feb. 1990.
[33] J. Huang, *Nonlinear Output Regulation: Theory and Applications*. Philadelphia, PA, USA: SIAM, 2004.
[34] I. A. Shkolnikov and Y. B. Shtessel, "Tracking controller design for a class of nonminimum-phase systems via the method of system center," *IEEE Trans. Autom. Control*, vol. 46, no. 10, pp. 1639–1643, Oct. 2001.
[35] I. A. Shkolnikov and Y. B. Shtessel, "Tracking in a class of nonminimum-phase systems with nonlinear internal dynamics via sliding mode control using method of system center," *Automatica*, vol. 38, no. 5, pp. 837–842, 2002.
[36] S. Devasia, D. Chen, and B. Paden, "Nonlinear inversion-based output tracking," *IEEE Trans. Autom. Control*, vol. 41, no. 7, pp. 930–942, Jul. 1996.
[37] Q. Zou and S. Devasia, "Precision preview-based stable-inversion for nonlinear nonminimum-phase systems: The VTOL example," *Automatica*, vol. 43, no. 1, pp. 117–127, 2007.

Linqi Ye received the bachelor's and Ph.D. degrees in control science and engineering from Tianjin University, Tianjin, China, in 2014 and 2019, respectively.

Since September 2019, he has been a Postdoctoral Researcher with the Center for Artificial Intelligence and Robotics, Tsinghua Shenzhen International Graduate School, Tsinghua University, Shenzhen, China. From September 2017 to September 2018, he was a Visiting Scientist with Cornell University, Ithaca, NY, USA. From September 2016 to September 2017, he was a Visiting Scholar with the State University of New York at Buffalo, Buffalo, NY, USA. His research interests include control of aerospace and robotic systems.

Bailing Tian (Member, IEEE) received the B.S., M.S., and Ph.D. degrees in automatic control from Tianjin University, Tianjin, China, in 2006, 2008, and 2011, respectively.

He is currently an Associate Professor with the School of Electrical and Information Engineering, Tianjin University. He was an Academic Visitor with the School of Electrical and Electronic Engineering, University of Manchester, Manchester, U.K., from June 2014 to June 2015.

Houde Liu (Member, IEEE) received the bachelor's degree in automation from the Huazhong University of Science and Technology, Wuhan, China, in 2007, and the master's and Ph.D. degrees in control science and engineering from the Harbin Institute of Technology, Harbin, China, in 2009 and 2014, respectively.

Since February 2014, he has been currently an Associate Researcher with the Center for Artificial Intelligence and Robotics, Graduate School at Shenzhen, Tsinghua University, Shenzhen, China. His research interests include modeling, control, and robotic systems.

Qun Zong (Member, IEEE) received the B.S., M.S., and Ph.D. degrees in automatic control from Tianjin University, Tianjin, China, in 1983, 1988, and 2002, respectively.

He is currently a Professor with the School of Electrical and Information Engineering, Tianjin University, where he is the Director of New Aircraft Guidance and Control Center, Ministry of Education.

Prof. Zong also serves as an editorial board member for several scientific journals.

Bin Liang (Senior Member, IEEE) received the bachelor's and master's degrees in control engineering from the Honors College of Northwestern Polytechnical University, Xi'an, China, in 1989 and 1991, respectively, and the Ph.D. degree in control engineering from the Department of Precision Instrument, Tsinghua University, Beijing, China, in 1994.

From 1994 to 2007, he held his positions as a Postdoctoral Researcher, an Associate Professor-Level Researcher, a Professor-Level, and an Assistant Chief Engineer with the China Aerospace Science and Technology Corporation, Beijing. Since 2007, he has been a Professor with the Department of Automation of Tsinghua University. His research interests include modeling and control of robotic systems.

Bo Yuan (Senior Member, IEEE) received the B.E. degree in computer science from the Nanjing University of Science and Technology, Nanjing, China, in 1998, and the M.Sc. and Ph.D. degrees in computer science from the University of Queensland (UQ), Brisbane, QLD, Australia, in 2002 and 2006, respectively.

From 2006 to 2007, he was a Research Officer on a project funded by the Australian Research Council with UQ. He is currently an Associate Professor with the Division of Informatics, Graduate School at Shenzhen, Tsinghua University, Shenzhen, China, where he is a member of the Intelligent Computing Lab. His research interests include intelligent computing and pattern recognition.